ACS APPLIED MATERIALS & INTERFACES

Research Article

www.acsami.org

Mechanical Characterization of Ultrasonically Synthesized Microbubble Shells by Flow Cytometry and AFM

Francesca Cavalieri,[†,‡] James P. Best,[§] Camilo Perez,[#] Juan Tu,[⊥] Frank Caruso,[§] Thomas J. Matula,*[,#] and Muthupandian Ashokkumar*[,†]

[†]School of Chemistry, The University of Melbourne, Parkville, Melbourne, Victoria 3010, Australia

[#]Center for Industrial and Medical Ultrasound, Applied Physics Laboratory, University of Washington, Seattle, Washington 98105, United States

[§]Department of Chemical and Biomolecular Engineering, The University of Melbourne, Parkville, Melbourne, Victoria 3010, Australia

[‡]Dipartimento di Scienze e Tecnologie Chimiche, Università di Roma Tor Vergata, 00173 Roma, Italy

[⊥]Key Laboratory of Modern Acoustics of Nanjing University, Ministry of Education Nanjing, Jiangsu, 210093 People's Republic of China

Supporting Information

ABSTRACT: The mechanical properties of the shell of ultrasonically synthesized lysozyme microbubbles, LSMBs, were evaluated by acoustic interrogation and nanoindentation techniques. The Young's modulus of LSMBs was found to be 1.0 ± 0.3 MPa and 0.6 ± 0.1 MPa when analyzed by flow cytometry and AFM, respectively. The shell elasticity and Young's modulus were not affected by the size of the microbubbles (MBs). The hydrogel-like protein shell of LSMBs offers a softer, more elastic and viscous interface compared to lipid-shelled MBs. We show that the acoustic interrogation technique is a real-time, fast, and high-throughput method to characterize the mechanical characteristics of air-filled microbubbles coated by a variety of materials.

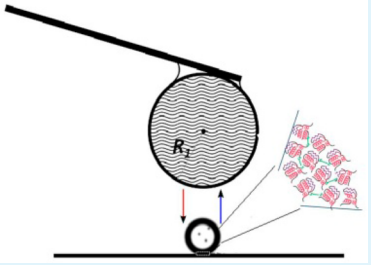

KEYWORDS: *acoustic cavitation, lysozyme, microbubbles, shell elasticity, flow cytometry, atomic force microscopy*

1. INTRODUCTION

Microbubbles, MBs, are gas bubbles stabilized by a protein or lipid shell, used in diagnostic imaging.[1−3] Commercially available thin phospholipid- (Definity, SonoVue) and albumin-shelled (Optison) MBs are currently used in clinical imaging. MBs have also been developed for targeted imaging and delivery of drugs.[4] The design and characterization of the physicochemical properties of MBs' shells are crucial because the composition of the shell (i) provides stability during administration and circulation through the vasculature, (ii) greatly affects the MBs' response to ultrasound, and (iii) provides a backbone for conjugation of ligands and drugs. Biopolymer-shelled micro and nanobubbles have been synthesized by high intensity ultrasound-induced emulsification and cross linking of lysozyme and other thiolated biopolymers in aqueous solutions.[5−8] In the process of the ultrasonic formation of LSMBs, lysozyme assembles at the air−liquid interface and forms a hydrogel-like structure stabilized by both newly formed intermolecular disulfide crosslinks and β-sheet domains.[2] The diameter and shell thickness of LSMBs, measured by optical and scanning electron microscopy over a set of 200 MBs are 2.5 ± 0.5 μm and 150 ± 30 nm, respectively.[7] Compared to the commercial products based on lipid shells and perfluoro gases microbubbles,[4] thick LSMBs offer many structural and functional advantages. Large scale production of relatively monodispersed and stable micro- and nanometer sized LSMBs is possible using the flow-through sonication technique without the use of perfluorocarbon gases.[8] LSMBs bear an intrinsic antimicrobial activity,[2] biodegradability and biocompatibility,[9] they are highly stable in aqueous suspensions at room temperature up to two years and possess echogenic properties for ultrasound contrast imaging.[8] The thick protein shell provides a platform for versatile functionalization with nucleotides, proteins[9] and gold nanoparticles.[10] In addition, it has been shown that LSMBs are readily internalized and degraded in SKBR3 breast cancer cells.[11] The emerging challenge is the design of therapeutic MBs that can potentially be transported across vascular walls (extravasation), and move through the tumor's interstitium. The rigidity and elastic modulus of micro- and nanobubbles have been found to tremendously affect circulation lifetime and biodistribution.[12] Softer particles (bubbles) in general circulate longer in vivo, evade immune system phagocytosis and pass through narrow microchannels.[13,14] Cellular internalization and trafficking of MBs are also dependent on the particle's elastic modulus.[15] The precise control over the mechanical properties of MBs' shells will lead to the understanding as to how stiffness and deformability of MBs affect circulation lifetime, biodistribution,

Received: July 29, 2013
Accepted: October 14, 2013
Published: October 14, 2013

cellular interaction and adhesion to immune-system cells. The stiffness or rigidity of the shell depends on material composition, porosity, and the shell thickness. To characterize the stiffness and elastic modulus of lipid and polymer MBs, AFM[16,17] and flow cytometry[18] have been recently used. Nanointerrogation of MBs using AFM coupled with a thin-shell theory for small deformations allows for the estimation of the Young's modulus. AFM offers several advantages, as a wide range of forces (from tens of pico to microNewtons) can be applied and deformations in the orders of nanometers detected on individual MBs in a suspension. Thin shelled (<30 nm) MBs made from a stiff synthetic polymer, poly(lactide), have a shell stiffness and a Young's modulus of approximately 1−7 N/m and 1−19 GPa, respectively, when analyzed by AFM.[19] The Young's modulus of commercial lipid coated MB shells, quantified using AFM nanoindentation in conjunction with elastic membrane theory is 19 ± 9 MPa, whereas a value of 133 ± 59 kPa was obtained using Hertzian mechanics for an equivalent homogeneous sphere.[16] Discrepancies between the two models occurred because of the intrinsic difficulties in applying Hertzian theory to the extremely thin shells under investigation. Additionally, shell stiffness of phospholipid coated MBs was also estimated using acoustic interrogation of the shells, and an average shell elasticity of 0.5−0.7 N/m was deduced.[18] The acoustic interrogation of microbubbles using flow cytometry was developed for phospholipid shells. We have investigated whether this technique can be considered as a versatile method for characterizing a variety of MBs, such as polymer-shelled MBs. In this work, we show for the first time to our knowledge the suitability of flow cytometry to determine the rheological properties of biopolymer-shelled microbubbles. We compare and discuss our results with previous studies performed on lipid-shelled MBs. In addition, we compare the mechanical characteristics of LSMBs determined by both flow cytometry and AFM.

2. EXPERIMENTAL SECTION

2.1. Materials. Tris buffer (tris(hydroxymethyl)amino methane), lysozyme from hen egg white, and DL-dithiothreitol (DTT), were purchased from Sigma−Aldrich (USA). Milli-Q filtered water (18 MΩ·cm) was used to prepare all solutions.

2.2. Synthesis and Characterization of Lysozyme-Shelled Microbubbles, LSMB. LSMBs were synthesized as described previously.[11] Lysozyme (5% w/v) was denatured in 50 mM Tris−HCl (pH 8.3) buffer for 2 min using 120 mM DTT. A 3 mm diameter microtip of a high-intensity ultrasonic horn (20 kHz, Branson) was positioned at the air−water interface and operated at an acoustic power of 160 W cm^{-2} for 30 s to obtain LSMBs. The mixture was then left standing for a few hours for LSMBs to float to the surface of the liquid. The excess DTT and the residual protein were repeatedly (5 times) washed off with Milli-Q water. The diameter and shell thickness of LSMBs were measured by optical and scanning electron microscopy over a set of 200 MBs.[7] The microbubble shell thickness was measured from the cross-section of the microbubble shell obtained from SEM images. The microbubble samples were frozen in liquid nitrogen and broken by a gentle "tap" using a spatula to expose a fresh cross-section of the shell.

2.3. Flow Cytometry Setup. The mechanical properties of the shell of LSMBs were measured using a modified flow cytometer. Details of the flow cytometer can be found in the literature.[18] In brief, an InFlux Cell Sorter (BD Biosciences, San Jose, CA) was modified to include a custom-made square quartz flow cell (Hamamatsu Photonics, Japan) with a 200 μm flow channel as a measurement chamber in place of the standard nozzle and fluid jet. Acoustic coupling to the carrier sheath fluid and LSMB samples occurred through a 1.0 mm thick piezoelectric element that was bound to one side of the flow cell with epoxy. The source signal to acoustically drive the flow cell assembly was generated by in-house made equipment: a function generator (HP 33120A, Agilent Technologies, Palo Alto, CA) connected to an RF amplifier (A150, ENI, Rochester, NY) though an RF step attenuator (837 Attenuator, Kay Elemetrics Corp, Lincoln Park, NJ). The PZT was driven with continuous wave sinusoidal voltages, leading to a variable pressure within the sensing region (ROI) of the cytometer. PMT signals were digitized by a 12 bit PXI-5105 at 25 MHz (National Instruments, Austin, TX) for analysis. For the purpose of characterizing the LSMBs in this study, we used the flow cytometer's side scatter optical path as described in our previous work on MB characterization.[18] The optical source was a 500 mW 488 nm laser (Sapphire 488-500, Coherent Inc., Santa Clara, CA). PMT signals were routed to a custom high bandwidth (-6 dB at 5 MHz) current to voltage converter and logarithmic preamplifier similar to that described by Shapiro.[20] Custom built Labview (National Instriments, Austin, TX) software was used to control the side scatter PMT gain setting. A National Instruments PXI data acquisition system was used for pulse digitization and storage. The flow cytometer PMT voltage output was converted to radii using Mie scattering theory. A modification of Mie scattering theory, applicable to a coated sphere, was first developed by Aden and Kerker[21] and later applied to coated bubbles by Marston et al.[22,23] Our implementation of the model for MBs is based on the equations in a book by Bohren and Huffman.[24] Normally, separate scattering coefficients should be applied to the shell and gas to calculate the relative scattering intensity from MBs.[25,26] However, the scattering features of small microbubbles of approximately 100 nm thick are almost identical to that of free gas bubbles,[27] thus the shell of our microbubbles can be neglected in the calculations. A typical calibration curve is shown in (Figure 1SI in the Supporting Information).

For this experiment, the applied frequency was 1.2 MHz. We inserted a FOPH hydrophone, but were unsuccessful at relying on the pressure reading due to the small size of the channel and possible contact with the fiber. The pressure amplitude was then obtained using the following procedure: the driving pressures were measured as voltage amplitudes from the function generator (V_a). We fitted the initial experimental pressure $P_a = kV_a$, where k is a scale value with the units of kilopascals per millivolt. The value of k was thus treated initially as a fitting parameter. After several numerical iterations with different data sets, this parameter converged to a value of 0.1 kPa/mV. In all subsequent experiments, we measured the pressure by applying this fitted calibration constant to the voltage signals. That is, knowing the applied voltage, and having found the constant k = 0.1 kPa/mV through iteration, the applied pressure can be determined. That leaves two unknown parameters, the shell viscosity and shell elasticity. Data processing to obtain elasticity and dilatational viscosity (χ (N/m) and κs (kg/s)) is described in the Supporting Information.

2.4. AFM Force Spectroscopy Measurements. Force measurements were performed using a Nanowizard II AFM coupled with a BioCell sample stage (JPK Instruments AG, Berlin, Germany). Measurements were performed using a colloidal probe AFM technique, where the cantilever was prepared by carefully immobilizing a glass bead (diameter 30−50 μm, Polysciences Inc, USA) onto the end of a tipless silicon cantilever (CSC12, Mikromasch, Estonia) using a 2-component epoxy adhesive (Selleys super strength, Australia), and the AFM as a micromanipulator. Before bead adhesion, the spring constant of the cantilever was determined using the thermal noise method. For the measurements, a 24 mm diameter round glass slide was used in the BioCell, and the glass substrate and cantilever were washed using 30% iso-propanol and cleaned using reactive oxygen plasma for 3 min (O_2 flow rate 0.1 L/min, 29.6 W, 300 mTorr, Harrick Plasma, USA) before measurement. The cleaned substrate was positioned at the top of a MB solution for 30 s to allow for positively charged LSMB surface attachment, and was then loaded into the BioCell and 500 μL of Milli-Q water was added. The AFM head was connected to a Leica DMI 4000B optical microscope set-up with a 40× objective (Leica Microsystems GmbH, Wetzlar, Germany), which allowed for optical visualisation, and importantly the alignment of the centre of the colloidal probe with the apex of the MBs for uniaxial

deformation. Typical compression/retraction cycles were performed using a constant piezo velocity of 625 nm/s.

Collected force spectra were analyzed using JPK data processing software. A baseline was firstly subtracted from the noncontact z-range of the force-displacement data, a probe/surface contact point then assigned, and the effect of cantilever bending subtracted to result in force−deformation ($F-\delta$) data from tip-sample separation data. The particle stiffness (k) was evaluated as the force−deformation gradient over the initial 20 nm of deformation. The Young's modulus (E_Y) was determined using the Hertz relationship for a spherical indenter on a spherical particle (as described in the main text), modelled over the first 40 nm of deformation. The Poisson's ratio was assumed to be 0.5, a reasonable value for an incompressible isotropic elastic material. In order to present representative k and E_Y values for the LSMBs, the force curves for 14 separate MBs were analyzed. Additionally, EMT and the Reissner model were used to verify the Hertzian E_Y value. Equations 2 and 3 were used with the shell stiffness to provide an estimate of the E_Y over 20 nm of deformation.

3. RESULTS AND DISCUSSION

Stable LSMBs were prepared using a well-established ultrasonic method, as described in our previous study.[11] The mechanism responsible for the formation of LSMBs was previously elucidated.[5,10] In brief, two ultrasound-induced phenomena are involved in the process: emulsification and cavitation (see Figure 2SI in the Supporting Information). The emulsification depends on the shear forces generated by the collapse of cavitation bubbles. In the second step, the cross-linking between the protein aggregates is induced by the HO_2 radicals generated during the acoustic cavitation

A custom-made flow cytometer was recently developed by Matula and co-workers[18] for analyzing the mechanical properties of lipid-shelled MBs. We used this technique to characterize cross-linked protein-shelled MBs. A conventional flow cytometry unit coupled with an ultrasonic transducer was used, as shown in Figure 3SI in the Supporting Information. A small PZT transducer was added to the side of a custom-built quartz flow cell with a 210 μm flow channel. Individual MBs travelling through the flow channel scatter the incident laser light (see Figure 3SI in the Supporting Information). The scattered light is collected and focused onto a field stop, and then detected by a photomultiplier tube (PMT). As the LSMBs flow through the cell, the incident acoustic energy forces their radial motion. The instantaneous change in their size in response to the acoustic energy is characterized by a change in the scattering signal that could be detected by the PMT.

The rheological properties of LSMB shells depend upon the chemical and physical network of the lysozyme shell. The specific geometry of this network is determined by disulfide crosslinks, in addition to hydrophobic and β-sheet domains that hold the protein molecules together. The hydrogel-like architecture of the LSMBs exhibits viscoelastic properties imparted by the disulfide crosslinking and other intermolecular physical interactions. The dynamic acoustic interrogation of LSMBs allows for the determination of both elastic and viscous contributions. When the LSMBs transit through the acoustic "interrogation zone", a modulation in the scattering signal, as shown in Figure 1, is detected. Light scattering of LSMBs was modelled using Mie theory. The scattering features of MBs of ca.100 nm thick are almost identical to that of free gas bubbles,[27] thus the shell thickness of the MBs can be neglected in the calculations. From the scattering modulation, a low pass filter provides the initial radius of the bubble using calibration measurements shown in the Supporting Information (Figure 1SI). From the high-pass filtering of the same signal, we extracted the bubble oscillation data in order to obtain a radius versus time ($R-t$) calibration curve. An example of the best-fit $R-t$ curve and the corresponding best fit parameters are shown in Figure 1.

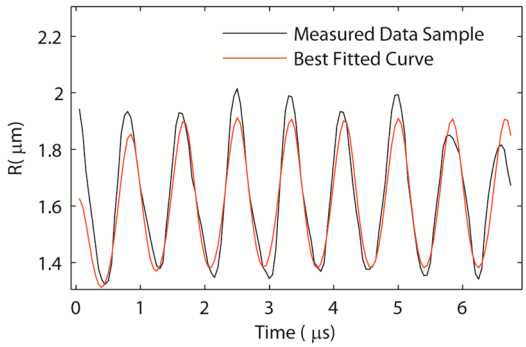

Figure 1. Sample best-fit data for LSMBs using Marmottant's model. The bubble was driven at 1.2 MHz and an acoustic pressure of 290 kPa. The best-fit shell parameters are χ = 0.12 N/m and κ_s = 9.0 × 10^{-8} kg/s, with R_0 = 1.63 μm.

To obtain the rheological parameters of the LSMB shells, we used Marmottant's dynamics equation (see eq 2 in the Supporting Information). Our study suggests that the $R-t$ curve acquired for LSMBs can be fitted well with the Marmottant's model for the estimation of shell parameters. Although developed for phospholipid shells, the results suggest that Marmottant's model may be used for LSMBs shells, at least as a first approximation. Using fits of the experimental $R-t$ data, the shell elasticity (χ) and the dilatational shell viscosity (κ_s) were extracted. As shown in Table 1 and Figure 2, the shell elasticity of the LSMBs is 0.15 ± 0.05 N/m, independent of the bubble radius, within experimental error. The elastic compression modulus can be related to shell elasticity by $\chi = Ed$, where d is the shell thickness (150 nm). As a fundamental

Table 1. Rheological Parameters of LSMBs and Commercially Available Contrast Agents

description	χ (N/m)	E_y (MPa)	κ_s (kg/s)
Definity	0.7 ± 0.2	175 ± 50	3×10^{-10} to 9×10^{-9}
SonoVue	0.5 ± 0.1	125 ± 25	5×10^{-9} to 3×10^{-8}
LSMBs	0.15 ± 0.05	1.0 ± 0.3	1×10^{-8} to 5×10^{-7}

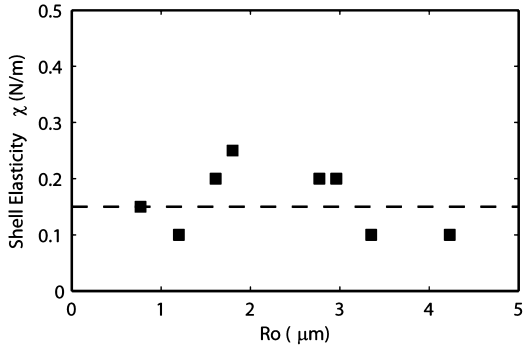

Figure 2. Relationship between LSMBs' shell elasticity and R_0. The shell elasticity was obtained by fitting the experimental $R(t)$ curves with Marmottant's model. The dashed line represents the mean of the elasticity values, χ = 0.15 ± 0.06 N/m.

surface physical constant of a material, χ should be independent of the total amount of shell material or its surface area. The results were compared with previous work for shell characterization[18] using commercial ultrasound lipid-shelled MBs (Definity and SonoVue). Significantly higher shell elasticity, 0.5−0.7 N/m, and elastic modulus, 125−175 MPa, were observed for lipid-shelled MBs.

This indicates that lipid assembly at the gas−water interface produces a stiffer membrane compared to the lysozyme hydrogel-like shell. Conversely, the covalent and physical networks of the protein offer a more elastic and softer interface. As for the shell viscosity, the shells of LSMBs are an order of magnitude more viscous than those of lipid MBs. The best-fit results suggest that the shell dilatational viscosity, κ_s, increases with an increase in the radius of the LSMBs (Figure 3). This is consistent with previous experimental observations

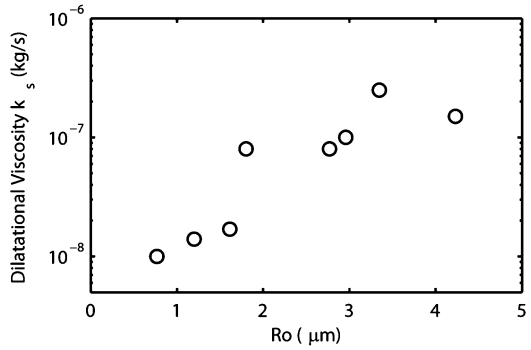

Figure 3. Relationship between LSMBs' shell dilatational viscosity and R_0.

on lipid-shelled MBs.[18] Van der Meer et al.[28] hypothesize that the variation of shell viscosity with R_0 should be attributed to rheological effects of shear thinning based on the dependence of shell viscosity on dilatational shear rate.

The decrease in the shell viscosity at the maximum shear rate indicates shear thinning. In Figure 4, the relationship between

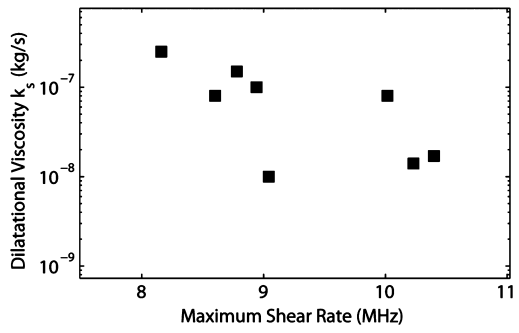

Figure 4. Relationship between the shell dilatational viscosity and maximum shear rate.

shell viscosity and the maximum shear rate, $\dot{R}/R$ calculated from the R-t data of protein shelled MBs is shown. We approximate the maximum shear rate as: $\dot{R}/R_{max} \approx 2\pi f_0 \Delta R_{max}/R_0$, where ΔR_{max} is the maximum amplitude of the radial oscillations, R_0 is the bubble radius, and f_0 the applied driving pressure. For a given driving pressure, the shell viscosity does indeed decrease with increasing maximum shear rate (Figure 4), in agreement with previously published data also using a single driving pressure.[18]

To validate the mechanical and rheological properties obtained for LSMBs using the flow cytometry technique, we performed force−indentation measurements using AFM.

For these measurements, a compressive force was applied using a large SiO_2 colloidal probe ($R_1 \approx 11.5$ μm) attached to a tipless cantilever.

Positively charged LSMBs (radius R_2) were immobilized to a negatively charged O_2 plasma-treated glass substrate to avoid lateral movement during compression. Measurements were performed using the method outlined in the Experimental Section. Figure 5 shows a typical force-deformation curve

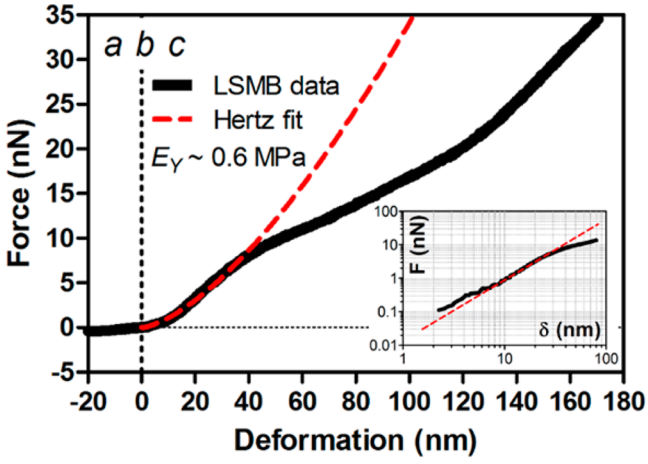

Figure 5. Representative force approach curve and Hertz fit (E_Y ca. 0.6 MPa) for LSMB indentation demonstrating (a) approach, (b) contact, and (c) deformation regimes, along with a corresponding log-log plot (inset, red line gradient 1.5).

obtained using low-spring-constant cantilevers ($k_c \approx 0.32$ N/m) for an immobilized LSMBs. Forces of up to 35 nN were applied in order to affect a deformation approximately equal to the LSMB shell thickness. A constant piezo velocity of 625 nm/s was utilized for all measurements. For all LSMBs studied, the shell elasticity was taken as the initial slope of the force−deformation curve (more than ca. 20 nm).

As the LSMBs are shell-structured materials, the Young's modulus is often elucidated using a Reissner model making use of thin-shell theory,[29] elastic membrane theory (EMT),[30,16] or even membrane contact theory for ideal gas compression.[31,32] For LSMBs with a diameter of 2.5 μm, the shell thickness (h) is *ca.* 150 nm, indicating that these systems are outside the range for thin shell models where the maximum limit is often considered as $h/R < 1/20$.[33] In addition, the membrane contact theory of Feng et al.[32] has only loosely been applied to pressurized capsule systems, as the model ignores fluid permeability through the shell and shell bending during compression, both of which are likely to occur during the deformation experiments. For cells, films and particles, a Hertz model (eq 1) is often employed for evaluation of the Young's modulus for small deformations, and has also recently been applied to investigate MB shells when treated as homogeneous spheres.[16] Indeed, Santos et al. compared the use of Reissner (eq 2), EMT (eq 3) and Hertz models for understanding the mechanical behaviour of phospholipid microbubbles under a compressive force.[16]

$$F^2 = \frac{16\delta^3 R_1 R_2 {E_Y}^2}{9(R_1 + R_2)(1 - \upsilon^2)^2} \quad (1)$$

$$F = \frac{\pi}{2\sqrt{2}} E_Y h^2 \sqrt{\varepsilon} + 4\pi E_Y h R_2 \varepsilon^3 \quad (2)$$

$$F = \frac{4(R_1 + R_2)\delta h^2 E_Y}{3\sqrt{1 - \nu^2} R_1 R_2} \quad (3)$$

The Hertz equation for a spherical indenter of radius R_1 effecting a deformation of a spherical object of radius R_2 is described in eq 1, where δ is the extent of the deformation for an applied force F, E_Y is the Young's modulus of the object material, and υ the Poisson's ratio of the material assumed here to be 0.5, which holds for an isotropic incompressible gel. It can be seen that for the Hertz model to apply, a linear relationship between force and deformation with a slope of 1.5 should be observed when the F−δ data is subjected to a logarithmic function. As can be seen from Figure 5 (inset), nanoindentation of LSMBs adheres to Hertzian theory, where for all collected data the mean log−log gradient is found to be 1.5 ± 0.1. We measured shell stiffness and Young's modulus values in the range of 71 ± 21 mN/m and 0.6 ± 0.1 MPa, respectively, with no significant variation with LSMB radius. This trend is in agreement with results obtained by flow cytometry. Results, as reported in Table 2, show that the Young's modulus was comparable using both methods.

Table 2. LSMB Mechanical Parameters Evaluated Using AFM

	Young's modulus (MPa)		
shell stiffness (mN/m)	Hertz	EMT	Reissner
71 ± 21	0.6 ± 0.1	0.6 ± 0.4	1.3 ± 0.6

To test the obtained Hertzian E_Y results, we additionally estimated the LSMB elastic modulus using EMT and the Reissner model, using eqs 2 and 3, respectively. The shell stiffness (F/δ), determined using linear regression analysis of the small deformation data, was incorporated with the relative deformation ($\varepsilon = \delta/2R_2$) to allow for E_Y elucidation. Compressive deformation modelling using EMT was found to provide an E_Y result similar to the Hertzian value (0.6 ± 0.4 MPa), as shown in Table 2. The elastic modulus determined using the Reissner model was higher than that using both Hertz and EMT modelling; however, it was also discussed that the LSMB systems studied here are outside the limits of conventional thin-shell theories. This is the first report, to our knowledge of using the Hertz model for the mechanical analysis of a MB shell, presumably because of the large shell thickness of the LSMBs and the deformation range analyzed.

Analysis of the ratio of bending to stretching components for the EMT, as previously outlined by Lulevich et al.,[30] demonstrates that bending resistances dominate in such systems. From Table 2, the shell elasticity evaluated using AFM is, however, lower than the cytometry result, likely a result of force analysis over a small deformation regime for the microbubble shell. From analysis of the force−deformation curves, it was found that a force hysteresis existed between approach and retract curves for all indentation experiments. This indicates that microbubble deformation over this range additionally contains a viscoelastic component, consistent with our reported flow cytometry results.

In conclusion, our results suggest that the use of flow cytometry in combination with force microscopy permits the extraction of physically meaningful viscoelastic parameters for LSMBs. These results give us confidence in the magnitude of the E_Y result using AFM and lead to the conclusion that flow cytometry provides a useful measure of the MB shell mechanics in such systems. The acoustic interrogation technique is a real-time, fast, and high throughput method to characterize the mechanical characteristics of microbubbles coated by a variety of materials.

■ ASSOCIATED CONTENT

Ⓢ Supporting Information

Flow cytometry calibration data (theoretical and experimental) is shown in Figure 1SI. A schematic diagram of LSMB preparation technique is shown in Figure 2SI. A schematic of the acoustic interrogation apparatus is shown in Figure 3SI. The modeling of the acoustic interrogation technique has also been described with appropriate references. This material is available free of charge via the Internet at http://pubs.acs.org/

■ AUTHOR INFORMATION

Corresponding Authors

*E-mail: masho@unimelb.edu.au. Fax: +61-3-93475180. Tel: +61383447090.

*E-mail: matula@apl.washington.edu.

Author Contributions

The manuscript was written through contributions of all authors. All authors have given approval to the final version of the manuscript.

Notes

The authors declare no competing financial interest.

■ ACKNOWLEDGMENTS

This work was supported by the Australian Research Council under the Australian Laureate Fellowship (F.C., 120100030), the University of Melbourne IPRS fellowship, and Victorian Government VIRS fellowship. We acknowledge the support for T.J.M. and C.P. provided by the Life Sciences Discovery Fund Authority #3292512 and the support for J.T. provided by National Natural Science Foundation of China #11074123.

■ ABBREVIATIONS

LSMBs, lysozyme-shelled microbubbles
AFM, atomic force microscopy

■ REFERENCES

(1) Cosgrove, D.; Harvey, C. *Med. Biol. Eng. Comput.* **2009**, *47*, 813−826.

(2) Cavalieri, F.; Zhou, M.; Ashokkumar, M. *Curr. Top. Med. Chem* **2010**, *12*, 1198−1210.

(3) Sirsi, S.; Borden, M. *Bubble Sci. Eng. Technol.* **2009**, *1*, 3−17.

(4) Ferrara, K.; Pollard, R.; Borden, M. *Annu. Rev. Biomed. Eng.* **2007**, *9*, 415−447.

(5) Cavalieri, F.; Ashokkumar, M.; Grieser, F.; Caruso, F. *Langmuir* **2008**, *24*, 10078−10083.

(6) Cavalieri, F.; Zhou, M.; Caruso, F.; Ashokkumar, M. *Chem. Commun.* **2011**, *47*, 4096−4098.

(7) Zhou, M.; Cavalieri, F.; Ashokkumar, M. *Soft Matter* **2011**, *7*, 623−630.

(8) Zhou, M.; Cavalieri, F.; Caruso, F.; Ashokkumar, M. *ACS Macro Lett.* **2012**, *1*, 853−856.
(9) Melino, S.; Zhou, M.; Tortora, M.; Paci, M.; Cavalieri, F.; Ashokkumar, M. *Amino Acids* **2012**, *43*, 885−896.
(10) Cavalieri, F.; Micheli, L.; Kaliappan, S.; Teo, B. M.; Zhou, M.; Palleschi, G.; Ashokkumar, M. *ACS Appl. Mater. Interfaces* **2013**, *5*, 464−471.
(11) Cavalieri, F.; Colone, M.; Stringaro, A.; Tortora, M.; Calcabrini, A.; Zhou, M.; Ashokkumar, M. *Part. Part. Syst. Charact.* **2013**, DOI: 10.1002/ppsc.201300025.
(12) Tao, S. L.; Desai, T. A. *J. Controlled Release* **2005**, *109*, 127−138.
(13) Merkel, T. J.; Jones, S. W.; Herlihy, K. P.; Kersey, F. R.; Shields, A. R.; Napier, M.; Luft, J. C.; Wu, H. L.; Zamboni, W. C.; Wang, A. Z.; Bear, J. E.; DeSimone, J. M. *Proc. Natl. Acad. Sci. U.S.A.* **2011**, *108*, 586−591.
(14) Doshi, N.; Zahr, A. S.; Bhaskar, S.; Lahann, J.; Mitragotri, S. *Proc. Natl. Acad. Sci. U.S.A.* **2009**, *106*, 21495−21499.
(15) Wang, J.; Byrne, J. D.; Napier, M. E.; DeSimone, J. M. *Small* **2011**, *14*, 1919−1931.
(16) Santos, E. B.; Morris, J. K.; Glynos, E.; Sboros, V.; Koutsos, V. *Langmuir* **2012**, *28*, 5753−5760.
(17) Grant, C. A.; McKendry, J. E.; Evans, S. D. *Soft Matter* **2012**, *8*, 1321−1326.
(18) Tu, J.; Swalwell, J.E.; Giraud, D.; Cui, W.; Chen, W.; Matula, T. *IEEE Trans. Ultrason. Ferroelectr. Freq. Control* **2011**, *58*, 955−963.
(19) Glynos, E.; Koutsos, V.; McDicken, W. N.; Moran, C. M.; Pye, S. D.; Ross, J. A.; Sboros, V. *Langmuir* **2009**, *25*, 7514−7522.
(20) Shapiro, H. M. *Practical Flow Cytometry*; Wiley: New York, 2003, 190−194.
(21) Aden, A. L.; Kerker, M. *J. Appl. Phys.* **1951**, *22*, 1242−1246.
(22) Marston, P. L. *Appl. Opt.* **1991**, *30*, 3479−3484.
(23) Marston, P. L.; Billette, S. C.; Dean, C. E. *Ocean Optics IX*; SPIE: Bellingham, WA, 1988; Vol. *925*, pp 308−316
(24) Bohren, C. F.; Huffman, D. R. *Absorption and Scattering of Light by Small Particles*; J. Wiley and Sons: New York, 1988.
(25) Marston, P. L. *Appl. Opt.* **1991**, 303479−303484.
(26) Marston, P. L.; Billette, S. C.; Dean, C. E. *Ocean Opt.* **1998**, *925*, 308−316.
(27) Guan, J. F.; Matula, T. J. *J. Acoust. Soc. Am.* **2004**, *116*, 2832−2842.
(28) Van der Meer, S. M.; Dollet, B.; Voormolen, M. M.; Chin, C. T.; Bouakaz, A.; de Jong, N.; Versluis, M.; Lohse, D. *J. Acous. Soc. Am.* **2007**, *121*, 648−656.
(29) Elsner, N.; Dubreuil, F.; Weinkamer, R.; Wasicek, M.; Fischer, F. D.; Fery, A. *Prog. Coll. Polym. Sci.* **2006**, *132*, 117−123.
(30) Lulevich, V.V.; Andrienko, D.; Vinogradova, O. I. *J. Chem. Phys.* **2004**, *120*, 3822−3826.
(31) Schmidt, S.; Fernandes, P. A. L; De Geest, B.; Delcea, M.; Skirtach, A. G.; Moehwald, H.; Fery, A. *Adv. Funct. Mater.* **2011**, *21*, 1411−1418.
(32) Feng, W. W; Yang, W. H. *J. Appl. Mech.* **1973**, *40*, 209−214.
(33) Gregory, R. D.; Milac, T. I.; Wan, F. Y. M. *SIAM J. Appl. Math.* **1998**, *59*, 1080−1097.